International Journal of Geo-Information

MDPI

Article

A Sensor Placement Strategy for Comprehensive Urban Heat Island Monitoring

Prasad Pathak [1,*], Pranav Pandya [1], Sharvari Shukla [2], Aamod Sane [3] and Raja Sengupta [4]

[1] Department of Physical & Natural Sciences, FLAME University, Pune 412115, Maharashtra, India
[2] Symbiosis Statistical Institute, Symbiosis International (Deemed University), Pune 411004, Maharashtra, India
[3] Department of Computing and Data Sciences, FLAME University, Pune 412115, Maharashtra, India
[4] Department of Geography and Bieler School of Environment, McGill University, Montreal, QC H3A 0B9, Canada
* Correspondence: prasad.pathak@flame.edu.in

Abstract: Urban heat islands (UHIs) increase the energy consumption of cities and impact the health of its residents. In light of the correlation between energy consumption and health and UHI variations observed at a local level within the canopy layer, satellite-derived land surface temperatures (LSTs) may be insufficient to provide comprehensive information about these deleterious effects. For both LST and air temperatures to be collected in a spatially representative and continuous manner, and for the process to be affordable, on-ground temperature and humidity sensors must be strategically placed. This study proposes a strategy for placing on-ground sensors that utilizes the spatial variation of measurable factors linked to UHI (i.e., seasonal variation in LSTs, wind speed, wind direction, bareness, and local climate zones), allowing for the continuous measurement of UHI within the canopy layer. As a representative city, Pune, India, was used to demonstrate how to distribute sensors based on the spatial variability of UHI-related variables. The proposed method may be helpful for any city requiring local-level observations of UHI, regardless of the climate zone. Further, we evaluate the placement of low-cost technology sensors that use LoRaWAN technology for this purpose, in order to overcome the problem of high costs associated with traditional in-situ weather stations.

Keywords: on-ground sensor placement; urban heat island; land surface temperature; local climate zones

check for updates

Citation: Pathak, P.; Pandya, P.; Shukla, S.; Sane, A.; Sengupta, R. A Sensor Placement Strategy for Comprehensive Urban Heat Island Monitoring. *ISPRS Int. J. Geo-Inf.* **2023**, *12*, 11. https://doi.org/10.3390/ijgi12010011

Academic Editors: Wolfgang Kainz and Godwin Yeboah

Received: 28 July 2022
Revised: 6 December 2022
Accepted: 21 December 2022
Published: 30 December 2022

1. Introduction

An urban heat island (UHI) is a phenomenon according to which the urban core of cities has been shown to be warmer than the surrounding rural areas, particularly at night [1,2]. Furthermore, as cities in developing countries (including those in India) experience rapid growth [3], the UHI phenomenon will exacerbate other deleterious environmental effects such as sustained heatwaves, increased energy consumption, and respiratory diseases [4–6]. Indeed, UHI intensity, as defined by the peak difference between temperatures in the urban core and the rural periphery, shows a significant correlation with population density [7]. This is because the UHI effect results primarily from urbanization, when natural surfaces (vegetation, grass, and open land) are replaced by human-made surfaces (asphalt, cement, and concrete) [8–10]. These human-made surfaces absorb more shortwave solar radiation than natural surfaces, and emit higher longwave radiation, resulting in elevated air and surface temperatures. Additionally, the development of urban canyons and anthropogenic heat also contributes to increased levels of UHIs [11]. While an increase in UHI intensity is anticipated, the methodologies that can be used to measure it are still in the process of being validated.

There are three major subcategories of UHI, based on the measurement method used and the height of the measurement: the surface UHI (SUHI), the canopy layer UHI (UHI_CL), and the boundary layer UHI (UHI_BL). Thermal remote sensing data are used

to determine the SUHI using measurements of the land surface temperature. This provides information about the difference in temperatures of the "skin" of surfaces in urban versus rural areas. With the assistance of weather stations or on-ground temperature sensors, the UHI_CL is calculated from ambient air temperatures within the canopy layer of urban and rural areas. The UHI_BL represents air temperatures beyond the canopy layer, and can be measured using high spectral resolution light detection and ranging technology (LIDAR) [12]. For this study, the UHI_BL was not an important factor.

The SUHI has been extensively studied because of the availability of thermal data from sensors such as Landsat, the moderate resolution imaging spectroradiometer (MODIS), and the advanced spaceborne thermal emission and reflection radiometer (ASTER) [13–16]. Additionally, these sensors have been used to observe changes in urban areas and UHIs over the years, and to measure their extent, as well as to incorporate interannual and seasonal variability. One important consideration is that the majority of these studies utilize data from the Landsat satellites, which mostly represent daytime SUHIs when the correlation with UHI_CLs has been shown to be weak. For our study, therefore, we rely on both daytime and night-time SUHI data obtained from MODIS satellites.

Further, satellite-derived thermal observations present the UHI phenomenon as a two-dimensional (2D) process. However, when one considers UHI_CLs, other factors come into play, which require consideration of three-dimensional (3D) factors at work within a city. As noted by Zhou et al. [17], the SUHI is not comparable to the UHI_CL, as the observation principles and altitudes are very different. Therefore, instead of relying on satellite data alone, the UHI_CL has traditionally been studied by using fixed or mobile weather stations [18]. For example, a relationship between urban canyons and the urban heat island effect has already been shown [8], emphasizing the 3D urban geometry responsible for forming and expanding the UHI_CL through urban development. Other studies have shown that the "skyview" factor is associated with the increased absorption of shortwave radiation, as well as a decrease in wind speed [9]. These studies have acknowledged the role of wind in carrying away longwave radiation. Thus, three-dimensional factors, such as urban geometry, wind speed, and wind direction, are all intrinsically linked to the UHI effect and result in variations in the UHI_CL. This is evident in the concept of local climate zones, which emphasizes the similarity of zones in terms of local land use, the type of built-up environment, and the number of vegetated areas with similar UHI_CL patterns [19]. Thus, the UHI_CL can only be observed through strategically placed air temperature sensors.

Despite the rapid expansion of cities in developing countries, most weather stations are sparse and distributed based on convenience, and do not adequately measure the parameters associated with the UHI_CL evenly throughout the city. As a result, they are unable to provide data that capture the spatial variations in the UHI_CL on a local scale [20]. This issue has been addressed in a few studies, which focus on the deployment of urban meteorological sensor networks. For instance, there are three levels of urban monitoring suggested by the World Meteorological Organization (WMO), namely: microscale (individual surfaces), local scale (neighborhoods), and mesoscale (city scale). This organization additionally provides specific guidelines, where a sensor must be placed at a site in the urban canopy layer that is surrounded by average or "typical" conditions for the urban terrain at a height similar to those used at non-urban sites. This assumes that the mixing induced by the flow around obstacles is sufficient to blend properties to form an urban canopy layer average on the local scale [21].

Moreover, the guidelines also specify the classification of urban climate zones for the selection of representative places and microclimates for sensors. These are similar to local climate zones, but are classified based on roughness, aspect ratio, and the percentage of built or impermeability measurements. Consequently, these guidelines form the basis of urban observations at a local level, but their derivation cannot be achieved without detailed fieldwork. The instrumentation requirements also necessitate sensors that are equivalent to standardized weather stations, which is an expensive proposition [21].

Muller et al. [22] reviewed numerous studies involving urban meteorological networks that followed WMO guidelines. To better understand the microclimatic conditions in urban areas, the guidelines stressed the importance of dense and spatially representative observations. As the study reviewed existing functional observation networks, it noted that they varied in scale, ranging from local to global. At the local level, only Oklahoma City had a functional network, whereas other urban areas were unable to sustain the network for a variety of reasons. They identified three main criteria as being important for the successful establishment and maintenance of these networks: (1) location (suitable and secure sites); (2) communication (data communication— wireless, LAN, radio); and (3) energy/power (for the sensors). The paper also underscored the fact that the cost of sensors is a factor that limits the number of sensors used; moreover, once the sensors are deployed, there are security issues directly related to the cost.

Two approaches have been used for the placement of sensors [23,24]. One approach is a carpet placement method that covers the entire study region, explicitly following range constraints [23]. The other approach is based on determining the path of least resistance for the signal using derivative information from the slope and environmental obstructions [24]. Mathematical approaches and tools such as the Voronoi diagram have been used to determine the voids in the carpet placement for denser placement strategy and void fixing [25]. Apart from mathematical and technical approaches, Smoliak et al. [26] capitalized on the help of volunteers to place 200 sensors in the Twin Cities Metropolitan Area, covering an area of 5000 km^2, in urban as well as peri-urban areas, based on personal experience and understanding. While this approach is interesting, it cannot be easily applied to other study areas.

In Mumbai, India, a study was recently conducted to determine the optimal number of meteorological sensors [27]. The objective of this study was to determine whether all 35 automatic weather stations in the area were necessary, or whether a smaller number of sensors would be sufficient to obtain similar spatio-temporal variability in the relevant hydrometeorological parameters. By analyzing the data generated from the existing 35 sensors, they performed principal component analysis and technique of order preference by similarity to arrive at an ideal solution. By using only 22 automatic weather stations, the researchers were able to predict the hazard zones for a river in Mumbai, thereby indicating the optimal locations of sensors by ranking them as either necessary or optional.

Of specific relevance to the present study is the classification of local climate zones, which has been used to group variations in the SUHI observed from satellite-based thermal sensors, and to correlate with on-ground air temperature sensor data [28,29]. However, no studies thus far have developed a specific methodology for the placement of low cost sensor that use LoRaWAN technology. It is clear that, in order to properly estimate the UHI_CL intensity with a limited number of sensors, efforts must be made to ensure that the on-ground air temperature sensors are placed in an optimal, spatially representative manner. This study proposes that on-ground sensors can be placed using a two-factor approach. One approach considers deriving the spatial variability of UHI-linked factors, estimated via the following four parameters: (a) local climate zones representing similar land use classes responsible for near-surface energy balance; (b) land surface temperature (LST) variations (daily and seasonal) to understand intra-urban pockets with high variability; (c) the normalized difference vegetation index (NDVI), representing vegetation cover, and (d) wind speed and wind direction, which are linked to heat dissipation and UHI intensity. The other approach is based on deciding the spatial distribution of sensors in identified areas based on technology-based choices (low-cost, continuous data capturing and transmission ability) as well as local conditions (public buildings, visibility of sensors to gateways). The objectives of the current study were to design an optimal and replicable sensor placement strategy for high-spatial-resolution sensing by: using the seasonal and annual variability of UHI-linked factors at the local level to identify the areas that would experience maximum variations in the LST; and (2) showcasing a method to distribute

a certain fixed number of sensors within the city based on the LST and causal factor variations, within budget constraints.

2. Materials and Methods

2.1. Study Area

Pune is the seventh most populous city in India and the second largest in the state of Maharashtra, with an estimated population of 7.4 million (as of 2020) [30] (Figure 1). The current area of Pune city is 243.84 sq. km, compared to a mere 125 sq. km. in 1951.

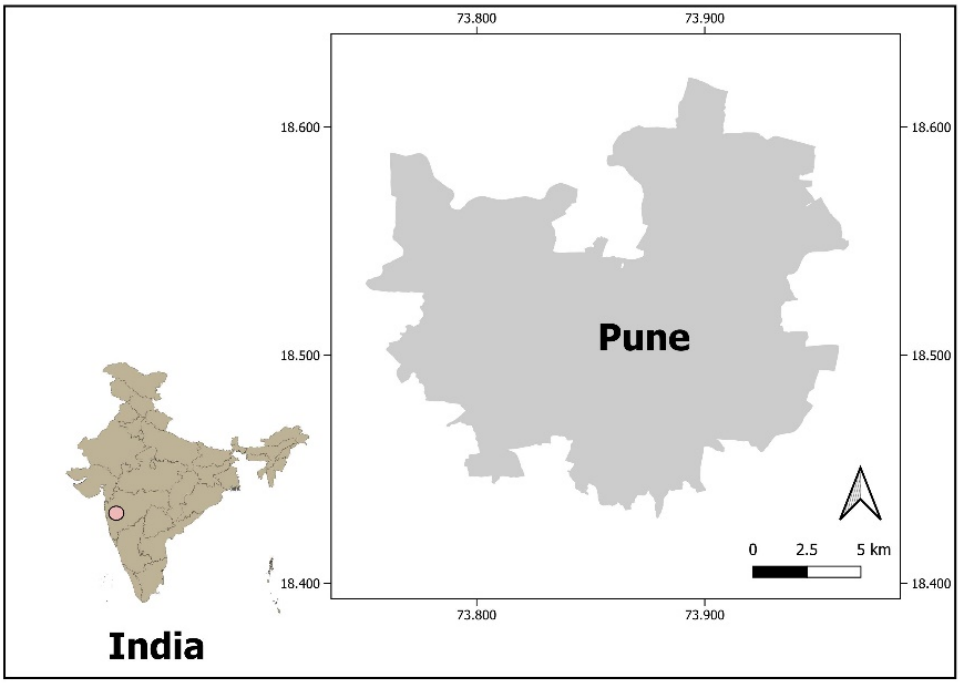

Figure 1. Location map of Pune.

According to the Indian Meteorological Department, Pune experiences four seasonal patterns: winter, pre-monsoon, southwest monsoon, and post-monsoon seasons (Table 1) [31]. Due to its elevation above sea level and proximity to the Western Ghats, the climate in the city is moderate, with an average temperature ranging from 20 °C to 30 °C. During the summer/pre-monsoon months, between March and May, maximum temperatures range between 35 °C and 38 °C. The monsoon season occurs from June to October, with temperatures ranging from 25 °C to 27 °C during this season. There is a mild winter season that begins in November, with the temperature hovering around 29 °C during the day and below 13 °C during the night for most of December and January, often dropping as low as 5 °C or 6 °C. Pune has a moderate climate, similar to most Indian cities.

Table 1. Months of the year in different seasons experienced in Pune.

Season	Month Span	Month Count
Winter	January–February	2
Pre-monsoon	March–May	3
Southwest monsoon	June–September	4
Post-monsoon	October–December	3

Note: specifications from the Indian Meteorological Department were used for data classification.

2.2. Data Sources

A total of seven causal factors (as well as the spatial resolution, source, and duration of the factors), as derived from five satellites (Table 2), were examined to determine suitable locations for air-temperature sensors.

Table 2. Data sources used in the study.

Data Type	Satellite Sensors	Resolution	Source	Duration
LST—day	MODIS–Aqua & Terra	1000 m	NASA	24 months (January 2019 to December 2020)
LST—night	MODIS–Aqua & Terra	1000 m	NASA	
Enhanced built-up and bareness (EBBI)	Landsat 8	30 m	U.S. Geological Survey (USGS)	
Local climate zone (LCZ)				
Wind speed	Terra Climate ERA5	4638.3 m 27,830 m	NASA Copernicus Climate Change Service (C3S)	
Wind direction				

For the Land Surface Temperature (LST), MODIS provides four observations of the LST per 24 h with its Aqua and Terra satellites. The satellite with the MODIS sensor takes observations at 1:30 a.m. and 1:30 p.m. for Aqua and 10:30 p.m. and 10:30 a.m. for Terra [32–34]. The monthly aggregated product (MOD11A1) for the LST from MODIS was used with a spatial resolution of 1 km. The Google Earth Engine API was used to filter the product for cloud percentage (80%), image quality (0.9), the geographical bounds of the study area, and the date of acquisition (January 2019 to December 2020).

Similar to the LST, with respect to the *Normalized Difference Vegetation Index (NDVI)*, the monthly aggregate (NDVI band, T1_32DAY_NDVI) product from MODIS was selected using the Google Earth Engine for the same time period.

With the *Enhanced Built-up and Bareness Index (EBBI)*, areas with higher proportions of built-up areas and barren areas were highlighted, and the index calculated using Landsat data for the years 2019 and 2020. Using the Google Earth Engine, Landsat 8 data were processed and the monthly *EBBI* was derived using the following formula [35]:

$$EBBI = \frac{Band\ 5 - Band\ 4}{10\sqrt{Band\ 5 + Band\ 6}}$$

These data were approximated to the 1 km grid.

Local Climate Zones (LCZ) were derived using the guidelines created by the World Urban Database and Access Portal Tools (WUDAPT) [36]. Using Landsat 8 data, we identified training sites for relevant LCZs present in the city. These were stored and uploaded to the WUDAPT site as KML files. The site provided a JPEG image with an LCZ classification for the entire city. The accuracy of the LCZ was calculated to make sure that it was reliable and suitable for further analysis [37]. The image was further converted into a vector file (polygons).

Lastly, the next two factors were related to wind. *Wind speed* data were obtained from NASA's TerraClimate satellite at a resolution of 2.5 arc minutes. Wind direction data were obtained from ERA5, which is part of the Copernicus Climate Change Service (C3S). To match the resolution of the MODIS dataset, both of these datasets (wind speed and wind direction) were also approximated to a 1 km grid.

2.3. Methods

The first step involved dividing the city into grids of one square kilometer (i.e., the native resolution of MODIS data), thus producing 332 grids, and then processing the parameters specified in Table 2 to derive the modulus for each grid cell. We should note

that only the MODIS-derived modulus had a native resolution of 1 square kilometer. The other parameters had to be resampled using QGIS software to match this cell resolution. Thus, the wind speed and direction data were downsampled from 4 by 4 kms. Furthermore, an LCZ category was assigned to each pixel of this map on a proportional basis, i.e., for every 1 sq. km cell, the proportions of the different types of LCZ were calculated. Google Earth images were used to verify the accuracy of the map, and it was found to be 82% accurate (Figure 2).

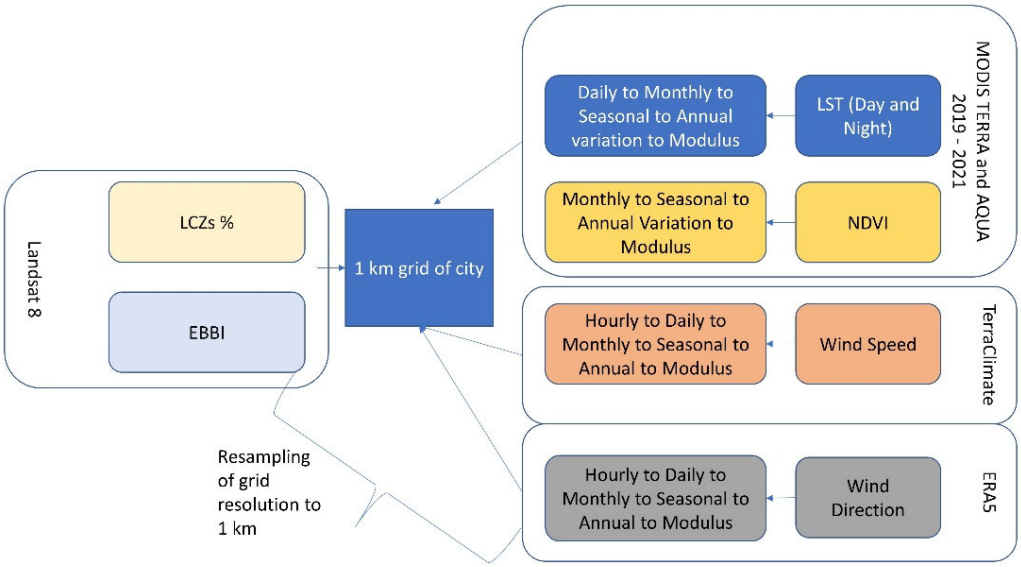

Figure 2. Deriving modulus for each of the datasets (Step 1).

Next, we ranked the grid cells according to the modulus variation of each parameter within them. In the case of a grid cell with the maximum modulus (seasonal and annual variation) of daytime LST, the value assigned to it would be 1, and if it was not that cell, the value assigned to the grid would be 0. Using this method, the annual and seasonal modulus values for each parameter were compared with each other, for each grid cell. During the final rank derivation, summation values for each of the LCZs obtained in the previous steps were used as weights. These were calculated by multiplying the LCZ proportions within each grid cell by these weights and adding them together. Our final output consisted of calculating the causal factor variability of each 1 × 1 km grid cell by rescaling the values obtained to 100. The assumption was that those cells with greater variability should be monitored more closely, with a greater distribution of sensors, than those with less variation (Figure 3).

Subsequently, each grid cell had a value between 0 and 100 as its rank, which indicated variability in the input parameters. For convenience, these cells were grouped into five categories, as shown in Table 3.

Table 3. Criteria for category assignment to the grid.

Category	Thermal Variability for Each Grid	Weight of Sensors per Grid
1	85% to 100%	5
2	70% to 85%	4
3	60% to 70%	3
4	40% to 60%	2
5	1% to 40%	1

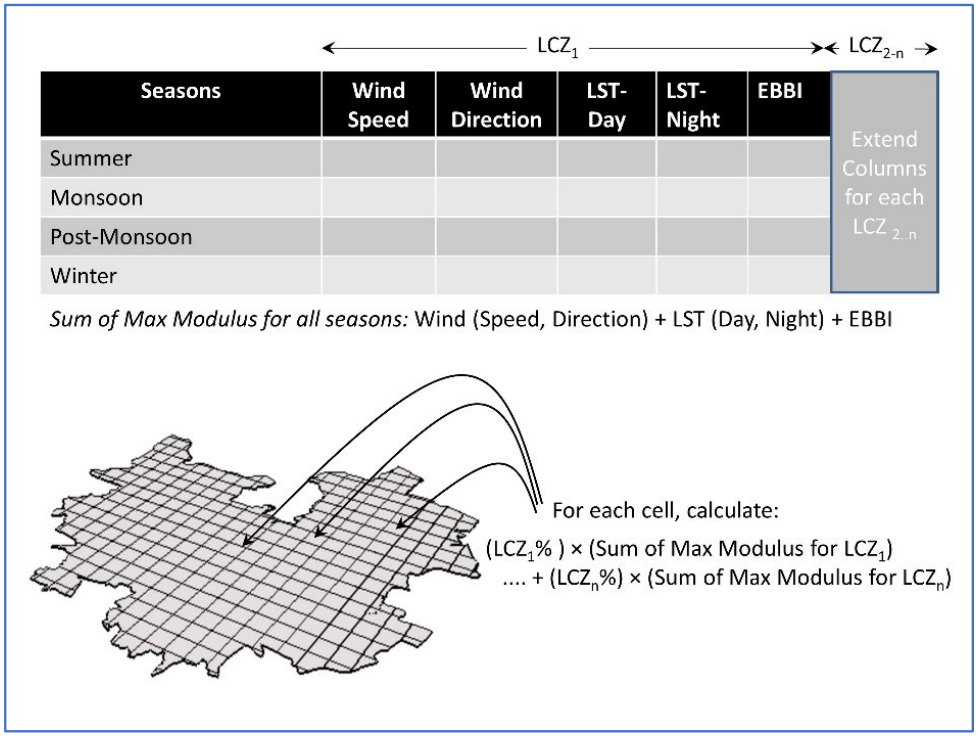

Figure 3. Ranking grids based on seasonal and annual variation (Step 2).

Because every study has a limited budget for sensors, it is important to estimate the density of sensors required to be placed within each 1 × 1 km grid cell. Therefore, the number of sensors required within each grid cell category was derived using the calculations depicted in Table 4. Furthermore, 500 is taken as the number of sensors required to be placed for our study, based on budgetary constraints. For example, at a cost of USD 50, 500 low-cost sensor technology (LoRaWAN) would be covered for a total budget of USD 25,000. These air temperature, surface temperature, and humidity sensors are an existing low-cost sensor technology with long battery life that are suitable for widespread deployment to obtain UHI_CL measurements. Because the number of sensors can be varied, Table 4 provides generic calculations that can be adjusted to accommodate any number of sensors.

Table 4. Criteria and number of sensors.

Category	Number of Grids in Each Category	Weight of Sensors (w) According to Criteria	Number of Sensors in Each Category	
1	n1	w1 = 5	n1w1/WS	[(n1w1/WS)] × Sensors/ZWS
2	n2	w2 = 4	n2w2/WS	[n2w2/WS] × Sensors/ZWS
3	n3	w3 = 3	n3w3/WS	[n3w3/WS] × Sensors/ZWS
4	n4	w4 = 2	n4w4/WS	[n4w4/WS] × Sensors/ZWS
5	n5	w5 =1	n5w5/WS	[n5w5/WS] × Sensors/ZWS
Total	N = Sum of n	W = 15	ZWS	

Here, n refers to the number of grids that fall into each category; w refers to the weights given to each category in Tables 2 and 3, i.e., [w1, w2, w3, w4, w5]; W refers to the sum of all weights given in Table 2; S refers to the total sensors available for use; ZWS refers to the sum of all rows above, i.e., [n1w1/WS, n2w2/WS, n3w3/WS, n4w4/WS, n5w5/WS].

The presence of public buildings/offices/schools and visibility was also considered. Public buildings were identified from the OpenStreetMap database, as they could be used for sensor/internet gateway placement and placed within each grid cell to check final

sensor placement possibilities. The criteria used were visibility and a distance of 500 m. For visibility analysis, the digital elevation model (CartoDEM) of the city was analyzed.

3. Results

3.1. Local Climate Zones

An LCZ classification was carried out based on the WUDAPT approach, as mentioned in the data pre-processing section, and an LCZ map was plotted for Pune, as shown in Figure 4. Pune city is dominated by an open midrise zone (LCZ 5). It is present in the cantonment area, which can be observed on the east side of the city center. The central area of the city has both open midrise (LCZ 5) and open lowrise (LCZ 6) zones. Occasionally, one can observe clusters of lightweight lowrises (LCZ 7). The eastern peripheral region of the city has a lot of open and barren area, classified as LCZ F. On the other hand, a few areas still have a good amount of vegetation, represented by LCZ A, such as that observed in the southern and western parts of the city. There are two rivers that merge to flow east near the city center.

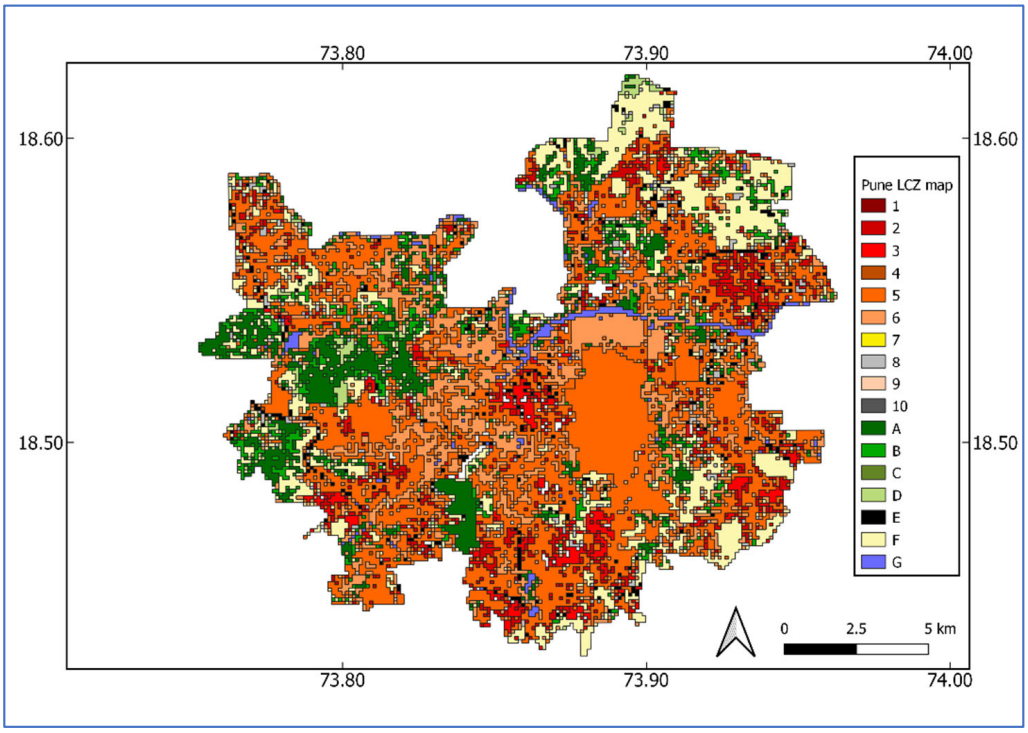

Figure 4. Local climate zones of Pune city as per WUDAPT with Landsat 8 (2020).

3.2. Grid Ranking Map of Pune

A map, whereby each grid is given a rank between 0 and 100, was the major output of this study. It shows areas with minimum to maximum variability in LST and wind, along with the bareness index and the proportion of LCZs associated with it (see Figure 5; for more details, refer to Figure 3 and Table 3). Thus, a score closer to 100 indicates those cells with a high variability in LST and wind at the seasonal and annual levels, as well as those that have a higher proportion of LCZs and vegetation, and the bareness conditions responsible for the variability. Therefore, it is recommended that these areas should be prioritized for sensor placement, whereas values closer to zero indicate cells with low variability in LST and the conditions responsible for it, suggesting that the density of sensors could be lower.

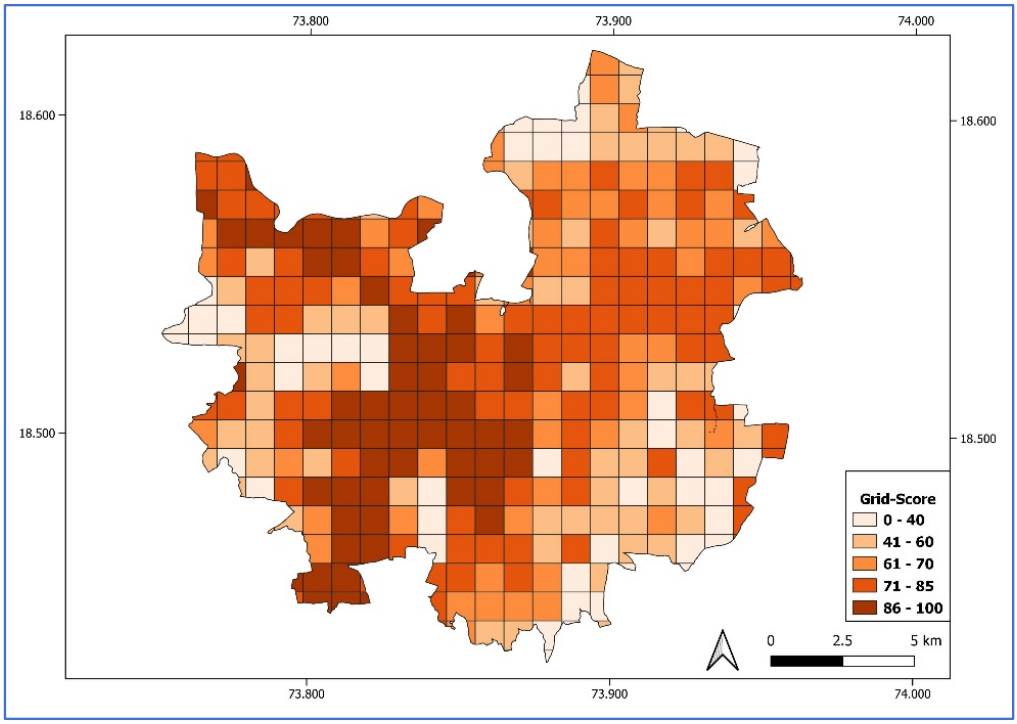

Figure 5. City divided into grids ranked from 0 to 100.

3.3. Sensor Placement

To determine the grids (based on ranking) and the number of sensors per category, we used the calculation illustrated in Table 4. Based on budgetary constraints discussed earlier, Table 5 summarizes the calculations and distribution of the number of sensors per category.

Table 5. Sensor count calculation for Pune.

Category	Number of Grids in Each Category	Weight of Sensors (w) According to the Criteria	Number of Sensors in Each Category			
1	61	w1 = 5	n1w1/WS	0.0407	[(n1w1/WS)] × Sensors/ZWS	144
2	101	w2 = 4	n2W2/WS	0.0539	[n2w2/WS] × Sensors/ZWS	190
3	60	w3 = 3	n3w3/WS	0.0240	[n3w3/WS] × Sensors/ZWS	85
4	60	W4 = 2	n4w4/WS	0.0160	[n4w4/WS] × Sensors/ZWS	57
5	50	W5 = 1	n5w5/WS	0.0067	[n5w5/WS] × Sensors/ZWS	24
Total	N = 332	W = 15	ZWS	0.1412	500	

Furthermore, modern sensor technology often uses radio signals (e.g., low-power wide-area networking, or LoRaWAN) to transmit data to a centralized server. This requires the installation of specialized gateways within a certain distance (e.g., 500 m) of the sensors. Based on the number of sensors and the gateway availability, the distribution per category may change, even when using the same method. The output of this method was visualized by overlaying the gateway locations and public buildings onto the ranked grids. Figure 6 depicts the locations that were identified for the installation of gateways. Government buildings such as hospitals, government offices, and schools were identified in various grids because these may be ideal locations for gateway installation and sensor placement. The cells in which sensors can be placed, based on the distance of the gateway, are indicated using the color-coded circles in the grids for the shortest distances from the identified government buildings or the closest gateway location. We should note that some grid cells with low scores have no locations identified where gateways could be placed; however,

the lack of gateways in this area is acceptable given that these regions do not have a high variability in the UHI_CL, and thus sensors need not be placed there.

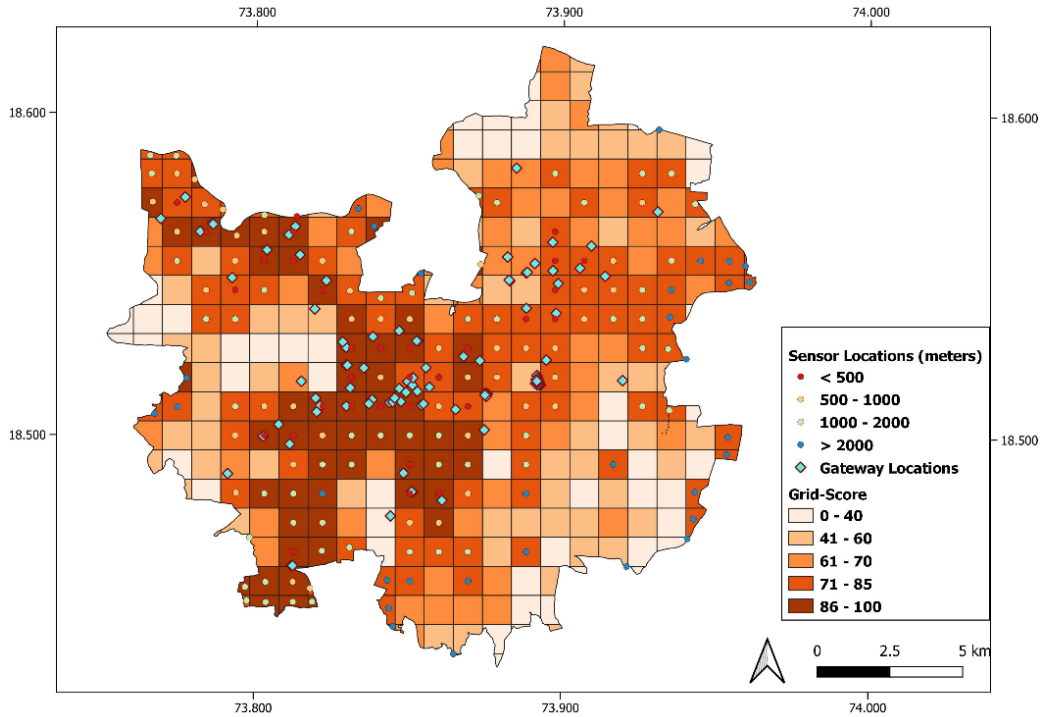

Figure 6. Color-coded network scheme for sensor placement.

4. Discussion

Urban Heat Island is a complex phenomenon because it relates to the balance of energy at the Earth's surface. The measurement of its component UHI_canopy layer is similarly complicated. Ideally, the UHI_CL needs to be monitored using an extremely dense network of sensors over a large coverage area. However, this is neither practical nor cost-effective. Instead, we developed a practical approach for deploying a feasible number (i.e., 500) of low-cost sensors that measure air and surface temperatures, and humidity. To do so effectively, it was necessary to develop an on-ground sensor placement strategy that would provide locations representing spatial variations within the UHI_CL. This was achieved by determining, from the available literature, the factors governing the UHI intensity that are easily captured by satellite data.

Due to the fact that the method presented is derived from publicly available satellite datasets (Landsat, MODIS, ERA5, and Terra Climate data) and is freely available through the Google cloud platform, it can be applied to any urban area. This ensures that the proposed placement algorithm can be tailored to each individual city. Furthermore, this approach can be applied to urban areas anywhere outside India, even to the cities in developed nations with varying climate zones, as it will generate a city-specific placement plan for sensors.

This study uses local climate zones (LCZs) as the basis for its analysis, since the LCZ method considers the heights of buildings, the distribution of surfaces, and the proportion of urban elements, according to the various forms of both human-made and natural elements. A study by Almeida et al. demonstrated that an LCZ-based sensor placement can successfully predict the UHI [30]. According to this study, the LCZ is capable of estimating the spatial patterns of the UHI, despite the lack of detailed field data for any city. However, additional parameters (such as wind speed and direction) enhance the information provided by LCZs, resulting in a more comprehensive understanding of the variability in urban health. In turn, this is the basis for developing a strategic sensor placement strategy.

The proposed approach preserved the details of the LCZ by keeping the proportion of LCZ classes per grid cell, despite rescaling the parameters to a grid size of 1 km. This approach is thus supported by the spatial composition on a finer scale of 30 m (i.e., the spatial resolution of the Landsat data from which LCZs were derived). In order to obtain daytime and night-time land-surface temperature observations, MODIS data were used, and all of the datasets were rescaled to match the spatial resolution of MODIS. As such, the proposed approach is a balanced approach, in which the analysis is conducted at a reasonable spatial scale of 1 square kilometer.

However, there are several limitations to this study. By identifying LCZs through the use of the WUDAPT method, which relies on satellite image interpretation, the proposed methodology avoids the monetary and time costs associated with detailed on-ground surveys, e.g., that required to calculate the urban climate zone. However, access to ERA5 data is required. Due to the charge associated with ERA5 historical data download, we limited the current analysis to the past two years. Furthermore, as Terra Climate satellites are able to capture atmospheric data (i.e., wind speed and direction) at a height of 10 m above the ground, the data do not match the height recommended by the World Meteorological Organization (WMO) for sensor placement (1.2 m). We decided to use wind data in this study, as these data are the best resource available to demonstrate variability, and Pune has a number of buildings that are higher than 10 m in height. As a result, we assumed that the wind data could be indicative of canopy layer conditions and could be used in conjunction with other surface and near-surface observations. Wind data can also be affected by changes in local topography. With high-resolution topography data, the proposed approach would be improved. Due to the cloud processing time and low topography variability in Pune, the current study did not consider this parameter.

5. Conclusions

We present a method for the strategic placement of on-ground air temperature sensors to measure the UHI_CL, which affects energy consumption and human health. Compared to traditional UHI measurement studies that use only satellite images, a complementary approach combining satellite images and local sensors results in a detailed UHI monitoring scheme. The sensor placement approach demonstrated in this study relied on satellite data to identify LCZs, as well as the spatial and temporal variability in local factors (surface temperature, wind speed, and wind direction) that result in urban heat islands. Furthermore, because the approach is based on the evidence of a surface UHI and is mathematically derived, personal biases are eliminated.

Using the spatio-temporal variability in the causal factors associated with thermal variability, we presented a placement scheme for 500 sensors across Pune. Assuming that the spatio-temporal variation in causal factors can serve as the basis for sensor placement planning, this demonstration can be modified according to the number of sensors that need to be placed.

In this study, we attempted to overcome the limitations of earlier sensor placement studies by utilizing satellite image variability to plan the placement scheme; this scheme can be applied to any study region, regardless of its growth patterns, and regardless of whether it is in a developing or a developed country.

In addition to taking potential financial burdens into account when placing sensors, the placement of sensors can also be determined based on the number of sensors available, and using the weights prescribed for each category of variable UHI. This paper presents theoretical research. The method will be further refined in the near future by establishing a sensor network based on the outputs from this paper.

Author Contributions: Pranav Pandya conceptualized the research idea and performed the analysis. Prasad Pathak contributed to the method, the analysis, and the preparation and editing of the manuscript. Raja Sengupta, Sharvari Shukla and Aamod Sane contributed to the analysis and to editing of the manuscript. All authors have read and agreed to the published version of the manuscript.

Funding: This work was funded by the Department of Science and Technology, the Government of India, and IC-IMPACTS, a Network Center of Excellence, Canada, under a grant titled "Improving Building Energy Demand Predictions in Smart Cities through Sensor Observations and Considerations of Landscape Characteristics" (DST/INT/CAN/P-05/20).

Data Availability Statement: The data used in this research were collected from MODIS, Terra-Climate (https://developers.google.com/earth-engine/datasets/catalog/IDAHO_EPSCOR_TERRACLIMATE?hl=en, accessed on 5 May 2022), ERA5 (https://developers.google.com/earth-engine/datasets/catalog/ECMWF_ERA5_DAILY?hl=en accessed on 15 April 2022), and Landsat series (https://developers.google.com/earth-engine/datasets/catalog/LANDSAT_LC08_C02_T2_L2 accessed on 15 April 2022).

Acknowledgments: We acknowledge the contribution made by Alexander Lam of McGill University, who provided technical suggestions for sensor placement requirements. We also acknowledge the contribution of the anonymous reviewers whose suggestions have improved the quality and clarity of the manuscript.

Conflicts of Interest: There are no conflict of interest to disclose.

References

1. Swain, D.; Roberts, G.J.; Dash, J.; Lekshmi, K.; Vinoj, V.; Tripathy, S. Impact of rapid urbanization on the city of Bhubaneswar, India. *Proc. Natl. Acad. Sci. India Sect. A Phys. Sci.* **2017**, *87*, 845–853. [CrossRef]
2. Oke, T.R.; Cleugh, H.A. Urban heat storage derived as energy balance residuals. *Bound. Layer Meteorol.* **1987**, *39*, 233–245. [CrossRef]
3. Arku, G.; Marais, L. Global south urbanisms and urban sustainability—Challenges and the way forward. *Front. Sustain. Cities* **2021**, *3*, 692799. [CrossRef]
4. Aflaki, A.; Mirnezhad, M.; Ghaffarianhoseini, A.; Ghaffarianhoseini, A.; Omrany, H.; Wang, Z.H.; Akbari, H. Urban heat island mitigation strategies: A state-of-the-art review on Kuala Lumpur, Singapore and Hong Kong. *Cities* **2017**, *62*, 131–145. [CrossRef]
5. Li, X.; Zhou, Y.; Yu, S.; Jia, G.; Li, H.; Li, W. Urban heat island impacts on building energy consumption: A review of approaches and findings. *Energy* **2019**, *174*, 407–419. [CrossRef]
6. Palecki, M.A.; Changnon, S.A.; Kunkel, K.E. The nature and impacts of the July 1999 heat wave in the midwestern United States: Learning from the lessons of 1995. *Bull. Am. Meteorol. Soc.* **2001**, *82*, 1353–1368. [CrossRef]
7. Oke, T.R. City size and the urban heat island. *Atmos. Environ.* **1973**, *7*, 769–779. [CrossRef]
8. Oke, T.R. The energetic basis of the urban heat island. *Q. J. R. Meteorol. Soc.* **1982**, *108*, 1–24. [CrossRef]
9. Grimmond, S.U.E. Urbanization and global environmental change: Local effects of urban warming. *Geogr. J.* **2007**, *173*, 83–88. [CrossRef]
10. Rizwan, A.M.; Dennis, L.Y.; Chunho, L.I.U. A review on the generation, determination and mitigation of Urban Heat Island. *J. Environ. Sci.* **2008**, *20*, 120–128. [CrossRef]
11. Hidalgo, J.; Masson, V.; Baklanov, A.; Pigeon, G.; Gimeno, L. Advances in urban climate modeling. *Ann. N. Y. Acad. Sci.* **2008**, *1146*, 354–374. [CrossRef]
12. Barlow, J.F.; Halios, C.H.; Lane, S.E.; Wood, C.R. Observations of urban boundary layer structure during a strong urban heat island event. *Environ. Fluid Mech.* **2015**, *15*, 373–398. [CrossRef]
13. Rajasekar, U.; Weng, Q. Spatio-temporal modelling and analysis of urban heat islands by using Landsat TM and ETM+ imagery. *Int. J. Remote Sens.* **2009**, *30*, 3531–3548. [CrossRef]
14. Sidiqui, P.; Huete, A.; Devadas, R. Spatio-temporal mapping and monitoring of Urban Heat Island patterns over Sydney, Australia using MODIS and Landsat-8. In Proceedings of the 2016 4th International Workshop on Earth Observation and Remote Sensing Applications (EORSA), Guangzhou, China, 4–6 July 2016; IEEE: New York, NY, USA, 2016; pp. 217–221.
15. Randolph, G.F.; Storper, M. Is urbanisation in the Global South fundamentally different? Comparative global urban analysis for the 21st century. *Urban Stud.* **2022**. [CrossRef]
16. Kaplan, G.; Avdan, U.; Avdan, Z.Y. Urban heat island analysis using the landsat 8 satellite data: A case study in Skopje, Macedonia. *Multidiscip. Digit. Publ. Inst. Proc.* **2018**, *2*, 358.
17. Zhou, D.; Xiao, J.; Bonafoni, S.; Berger, C.; Deilami, K.; Zhou, Y.; Frolking, S.; Yao, R.; Qiao, Z.; Sobrino, J.A. Satellite remote sensing of surface urban heat islands: Progress, challenges, and perspectives. *Remote Sens.* **2018**, *11*, 48. [CrossRef]
18. Oke, T.R. Canyon geometry and the nocturnal urban heat island: Comparison of scale model and field observations. *J. Climatol.* **1981**, *1*, 237–254. [CrossRef]
19. Stewart, I.D.; Oke, T.R.; Krayenhoff, E.S. Evaluation of the 'local climate zone'scheme using temperature observations and model simulations. *Int. J. Climatol.* **2014**, *34*, 1062–1080. [CrossRef]
20. Wang, K.; Jiang, S.; Wang, J.; Zhou, C.; Wang, X.; Lee, X. Comparing the diurnal and seasonal variabilities of atmospheric and surface urban heat islands based on the Beijing urban meteorological network. *J. Geophys. Res. Atmos.* **2017**, *122*, 2131–2154. [CrossRef]

21. Oke, T.R. *Initial Guidance to Obtain Representative Meteorological Observations at Urban Sites*; WMO/TD No. 1250; World Meteorological Organization: Geneva, Switzerland, 2004.
22. Muller, C.L.; Chapman, L.; Grimmond, C.S.B.; Young, D.T.; Cai, X. Sensors and the city: A review of urban meteorological networks. *Int. J. Climatol.* **2013**, *33*, 1585–1600. [CrossRef]
23. Curtin, K.M.; Qui, F.; Hayslett-McCall, K.; Bray, T.M. Integrating GIS and maximal covering models to determine optimal police patrol areas. In *Geographic Information Systems and Crime Analysis*; IGI Global: Hershey, PA, USA, 2005; pp. 214–235.
24. Argany, M.; Mostafavi, M.A.; Gagné, C. Context-aware local optimization of sensor network deployment. *J. Sens. Actuator Netw.* **2015**, *4*, 160–188. [CrossRef]
25. Argany, M.; Mostafavi, M.A.; Karimipour, F.; Gagné, C. A GIS based wireless sensor network coverage estimation and optimization: A Voronoi approach. In *Transactions on Computational Science XIV*; Springer: Berlin/Heidelberg, Germany, 2011; pp. 151–172.
26. Smoliak, B.V.; Snyder, P.K.; Twine, T.E.; Mykleby, P.M.; Hertel, W.F. Dense network observations of the Twin Cities canopy-layer urban heat island. *J. Appl. Meteorol. Climatol.* **2015**, *54*, 1899–1917. [CrossRef]
27. Ghosh, M.; Singh, J.; Sekharan, S.; Ghosh, S.; Zope, P.E.; Karmakar, S. Rationalization of automatic weather stations network over a coastal urban catchment: A multivariate approach. *Atmos. Res.* **2021**, *254*, 105511. [CrossRef]
28. Almeida, C.R.D.; Furst, L.; Gonçalves, A.; Teodoro, A.C. Remote Sensing Image-Based Analysis of the Urban Heat Island Effect in Bragança, Portugal. *Environments* **2022**, *9*, 98. [CrossRef]
29. Alexander, P.J.; Mills, G. Local climate classification and Dublin's urban heat island. *Atmosphere* **2014**, *5*, 755–774. [CrossRef]
30. Chandramouli, C.; General, R. *Census of India 2011—Rural Urban Distribution of Population, Provisional Population Total*; New Delhi Office of the Registrar General and Census Commissioner: New Delhi, India, 2011.
31. Arora, S.K.; Jha, B.; FAQ India Meteorological Department. India Meteorological Department. 2010. Available online: http://imd.gov.in/section/nhac/wxfaq.pdf (accessed on 3 August 2021).
32. Viana, C.M.; Oliveira, S.; Oliveira, S.C.; Rocha, J. Land use/land cover change detection and urban sprawl analysis. In *Spatial Modeling in GIS and R for Earth and Environmental Sciences*; Elsevier: Amsterdam, The Netherlands, 2019; pp. 621–651.
33. Maurer, J. Overview of NASA's Terra Satellite. 2001. Available online: http://www2.hawaii.edu/~{}jmaurer/terra (accessed on 20 February 2022).
34. NASA. MODIS Web. 2020. Available online: https://modis.gsfc.nasa.gov/about/specifications.php (accessed on 20 February 2022).
35. As-Syakur, A.R.; Adnyana, I.W.S.; Arthana, I.W.; Nuarsa, I.W. Enhanced built-up and bareness index (EBBI) for mapping built-up and bare land in an urban area. *Remote Sens.* **2012**, *4*, 2957–2970. [CrossRef]
36. Demuzere, M.; Kittner, J.; Bechtel, B. LCZ Generator: A web application to create Local Climate Zone maps. *Front. Environ. Sci.* **2021**, *9*, 637455. [CrossRef]
37. Huang, X.; Liu, A.; Li, J. Mapping and analyzing the local climate zones in China's 32 major cities using Landsat imagery based on a novel convolutional neural network. *Geo-Spat. Inf. Sci.* **2021**, *24*, 528–557. [CrossRef]